Process Safety and Environmental Protection 120 (2018) 339–347

Contents lists available at ScienceDirect

Process Safety and Environmental Protection

journal homepage: www.elsevier.com/locate/psep

Mechanothermal synthesis of Ag/TiO_2 for photocatalytic methyl orange degradation and hydrogen production

R. Saravanan [a], Devaraj Manoj [b], Jiaqian Qin [c], Mu. Naushad [d,*], F. Gracia [e], Adam F. Lee [f,*], Mohammad Mansoob Khan [g], M.A. Gracia-Pinilla [h,i]

[a] Escuela Universitaria de Ingeniería Mecánica (EUDIM), Universidad de Tarapacá, Avda. General Velásquez 1775, Arica, Chile
[b] Department of Physical Chemistry, University of Madras, Guindy Campus, Chennai, 600 025, India
[c] Metallurgy and Materials Science Research Institute, Chulalongkorn University, Bangkok 10330, Thailand
[d] Department of Chemistry, College of Science, Building#5, King Saud University, Riyadh, 11451, Saudi Arabia
[e] Department of Chemical Engineering, Biotechnology and Materials, University of Chile, Beauchef 851, 6th floor, Santiago, Chile
[f] School of Science, RMIT University, Melbourne VIC3000, Australia
[g] Chemical Sciences, Faculty of Science, Universiti Brunei Darussalam, Jalan Tungku Link, Gadong, BE 1410, Brunei Darussalam
[h] Universidad Autónoma de Nuevo León, Facultad de Ciencias Físico-Matemáticas, Av. Universidad, Cd. Universitaria, San Nicolás de los Garza, NL, Mexico
[i] Universidad Autónoma de Nuevo León, Centro de Investigación en Innovación y Desarrollo en Ingeniería y Tecnología, PIIT, Apodaca, N.L., Mexico

ARTICLE INFO

Article history:
Received 26 June 2018
Received in revised form 8 September 2018
Accepted 13 September 2018
Available online 15 September 2018

Keywords:
TiO_2
Silver
Photocatalysis
Hydrogen
Methyl orange

ABSTRACT

Photocatalysis offers a promising route to address the challenges of future energy production and anthropogenic environmental pollution. Here we demonstrated the synthesis of a high activity Ag/TiO_2 photocatalyst through a two-step, sol-gel and mechanothermal decomposition method employing a silver acetate precursor. Bulk and surface characterization revealed the formation of dispersed metallic silver nanoparticles (~9 nm diameter) decorating anatase crystallites (~14 nm) which stabilized a significant concentration of Ti^{3+} surface species. Synergy between silver and titania enhanced the photophysical properties, narrowing the band gap and suppressing charge-carrier recombination. Ag/TiO_2 exhibited good visible light activity and excellent stability over 3 cycles for the aqueous phase photocatalytic degradation of methyl orange dye (38 $\mu mol/h/g_{cat}$), and excellent hydrogen production from water splitting (910 $\mu mol/h/g_{cat}$).

1. Introduction

Global energy demand is predicted to rise more than 50 percent between 2013–2040, largely due to population growth and associated expansion of transportation, industrial, residential and commercial sectors (US Energy Information Administration, 2016). A parallel increase in the quantity and diversity of pollutants released into the environment is also predicted, due to an over-reliance on chemicals for agriculture and manufacturing and the concomitant release of contaminated waste. Photocatalysis offers a valuable approach to address both solar fuels production and environmental depollution (Khan et al., 2014a; Yan et al., 2013; Sivula and Krol, 2016; Wang et al., 2016; Tachibana et al., 2012; Ge et al., 2016a), with hydrogen generation via photocatalytic water splitting (Khan et al., 2014a; Yan et al., 2013; Sivula and Krol, 2016; Wang et al., 2016; Tachibana et al., 2012; Ge et al., 2016a). In regard of the environmental remediation, water pollution accounts for >840,000 fatalities annually worldwide, with 80% of associated contaminants arising from the discharge of toxic, organic compounds by industrial and agricultural processes (World Health Organization WHO, 2017). Organic azo dye such as methyl orange is difficult to treat by conventional bio- and/or physicochemical processing (Chan et al., 2009; Awual et al., 2015a,b; Awual and Hasan, 2015; Awual et al., 2016) and their concentrations can reach 500 ppm in textile effluents (Chequer et al., 2013). Advanced oxidation processes such as Fenton and photo-Fenton oxidation are promising solutions to their oxidative removal from wastewater but require significant quantities of H_2O_2 and are prone to metal leaching. Photocatalytic solutions to wastewater depollution are therefore desirable.

In recent years, solid state nanomaterials such as semiconductors, nanoparticles, nanowires, nanotubes, nanoporous, and hollow materials have found which have applications to energy and environment science, especially in photocatalysis (Khan et al., 2014a;

* Corresponding authors.
E-mail addresses: mnaushad@ksu.edu.sa (Mu. Naushad), adam.lee2@rmit.edu.au (A.F. Lee).

https://doi.org/10.1016/j.psep.2018.09.015
0957-5820/

Ge et al., 2016a). Such nanomaterials offer high surface areas, rapid charge transport and selective chemical transformations. For over three decades, titania has been the most widely used photocatalyst due to its high thermochemical stability, low toxicity, abundance, and conduction band energy which renders it suitable for oxidation processes (Khan et al., 2014a; Yan et al., 2013; Ge et al., 2016a; Luttrell et al., 2014), notably photodegradation of organic pollutants under UV irradiation. While compared with brookite and rutile phase of TiO_2, anatase phase show high catalytic performance because of oxidation and reduction potential favor for removal of contamination under UV illumination (Luttrell et al., 2014). However, the wide band gap and poor quantum efficiency of pure TiO_2 is a barrier to solar photocatalysis (Khan et al., 2014a; Yan et al., 2013; Ge et al., 2016a; Luttrell et al., 2014; Pelaez et al., 2012; Kumar et al., 2017), although diverse methods exist to engineer the physical/electronic structure and chemical composition of TiO_2 including through nanocomposite formation (Pelaez et al., 2012, 2012; Kumar et al., 2017) in order to utilize visible light. Ag/TiO_2 has shown potential for photocatalytic energy and environmental applications (Zhou et al., 2011, 2014; Ubonchonlakate et al., 2012; Hu et al., 2016; Gomes et al., 2017; Wang et al., 2013; Fei and Li, 2014; Lim et al., 2014; Wu et al., 2013; Ravishankar et al., 2015), including through plasmonic enhancement of dye sensitized solar cells (Lim et al., 2014); silver is particularly attractive due to its low toxicity to humans and visible surface plasmon resonance (Gomes et al., 2017; Zhou et al., 2014; Ubonchonlakate et al., 2012; Hu et al., 2016; Gomes et al., 2017; Wang et al., 2013; Fei and Li, 2014; Lim et al., 2014; Wu et al., 2013; Ravishankar et al., 2015). Ag/TiO_2 photocatalysts are typically synthesized through (thermos) chemical reduction, which hinders control over the resulting dimensions, composition and phase of the resulting material, hence new synthetic approaches desirable to elucidate the nature of active sites and synergy between components.

Herein, we report a new route for Ag/TiO_2 through a combined sol-gel and subsequent mechanothermal synthesis which obviates the need for a reduction step, and affords a simple and cost-effective route to high activity photocatalysts for the photocatalytic degradation of azo dyes, and production of hydrogen from water, under UV or/and solar irradiation.

2. Experimental

2.1. Materials

Titanium tetra isopropoxide (TTIP), isopropyl alcohol, citric acid, cetyltrimethyl ammonium bromide (CTAB), silver acetate, methanol and methyl orange (MO) were purchased from Sigma-Aldrich. All aqueous solutions were prepared using deionized water.

2.2. Catalyst synthesis

The synthesis procedure was followed by our pervious study (Saravanan et al., 2018). In short, the synthesis of the parent TiO_2 support and subsequent Ag/ TiO_2 catalyst is illustrated in Fig. 1. Porous TiO_2 was prepared by a sol-gel method as follows. A 1:5 ratio of TTIP solution was dissolved in isopropyl alcohol under continuous stirring (beaker A); simultaneously, 0.5 moL citric acid was dispersed in deionized water (beaker B). Subsequently, the citric acid solution was added dropwise to the TTIP solution resulting in colloidal gel formation. The gel was aged overnight, and then dried at 100 °C for 30 min in vacuo to yield a dry powder, and then calcined at 400 °C for 1 h to produce anatase TiO_2; this thermal processing treatment was determined by TGA analysis to ensure complete decomposition of the alkoxide precursor and titania crystallization. Silver doping of the parent TiO_2 followed a modified vapor evaporation method (Pan et al., 2001; Saravanan et al., 2013; Logvinenko et al., 2007). Silver acetate and TiO_2 were mixed in a 1:9 wt% ratio and ground for 3 h in an agate pestle and mortar, and then calcined at 400 C for 1 h to decompose the acetate, and slowly cooled (4 °C/min) to room temperature. X-ray fluorescence (XRF) confirmed the final Ag loading as 4 wt%.

2.3. Dye degradation

The photoactivity of Ag/TiO_2 was evaluated under UV and simulated solar irradiation for methyl orange (MO) degradation. The photocatalytic reactor and catalyst testing was done by following our previous reports (Saravanan et al., 2013, 2014). Experiments utilized either an 8 W Hg vapor lamp (365 nm), or a solar simulator (SCIENCETECH, model No: SF300B, along with AM 1.5 G filter). The illumination intensity of light irradiation at the sample surface was ~100 mW/cm^2 in both cases. An initial concentration of 5×10^{-5} M of MO dye was used to aid comparison with literature photocatalytic degradation studies of methyl orange, and being indicative of that encountered in waste water streams from the textile industry (Chequer et al., 2013). 500 mg of Ag/TiO_2 was mixed with 500 mL of dye solution in a 600 mL jacketed quartz reactor under constant stirring at 25 °C; this catalyst loading was chosen to aid comparison with our previous studies (Gupta et al., 2017) The catalyst slurry was equilibrated with the dye for 1 h in the dark prior to illumination, and then irradiated with either UV or solar light, and aliquots of the solution collected at regular intervals. Dye concentrations were measured following centrifugation of aliquots to remove residual catalyst, using UV–vis absorption spectroscopy. Before the photocatalytic experiment; the adsorption capability of the catalyst were carried and the result exhibited that the adsorption capacity of the catalyst is ~1–2% only. The adsorption value is separated from the photodegradation rate. Control photolysis experiments in the absence of photocatalyst showed negligible MO decomposition over the 80 min duration of experiments, while equilibration studies in the dark demonstrated that only 1–2 % of the initial dye adsorbed on the catalyst in the dark. Post-reaction, the spent catalyst was centrifuged, filtered and dried at 100 °C; XRF evidenced negligible silver leaching.

2.4. Hydrogen production

The photoactivity of Ag/TiO_2 was also evaluated under UV and simulated solar irradiation for hydrogen production by water splitting. The experimental protocol followed previous reports (Wu et al., 2013; Ravishankar et al., 2015; Gupta et al., 2017). In this study, we used 8 W Hg vapor lamp (365 nm) and solar simulator (SCIENCETECH, model No: SF300B, along with AM 1.5 G filter) for light source of irradiation activity. 200 mL of methanol:water mixture (1:1 by volume) and 100 mg of Ag/TiO_2 were mixed in a 250 mL jacketed photoreactor under constant stirring at 25 °C. The solution was degassed by purging with Ar gas prior to reaction. The reactor headspace was periodically sampled using a gas syringe and H_2 quantified by GC-gas chromatography (Perkin Elmer Autosystem) using a thermal conductivity detector.

2.5. Characterization

The structure of the as-prepared materials was analyzed by X-ray diffractometer (D5000 diffractometer, Siemens, USA) with Cu $K_{\alpha 1}$ ($\lambda = 1.5406$ Å) radiation operated at 40 kV and 30 mA (Saravanan et al., 2018). Diffractograms were collected in between 20° to 80° at room temperature with a step size of 0.02° and a scan rate of 0.5 s/step. Rietveld refinements of XRD patterns were executed using TOPAS software. Elemental analysis was performed

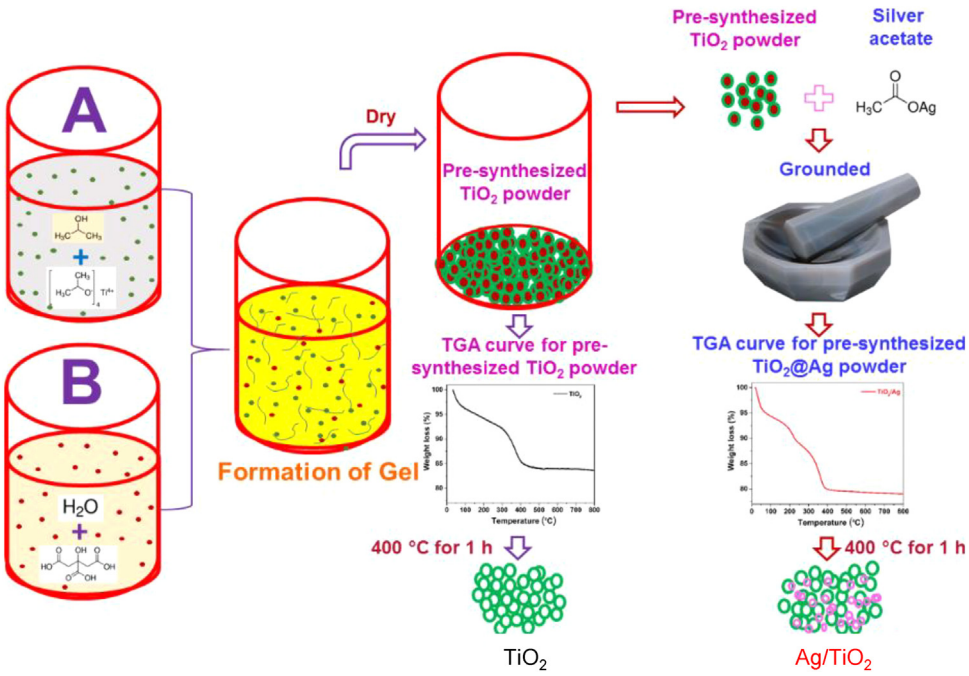

Fig. 1. Synthesis of porous TiO_2 and Ag/TiO_2.

by X-ray fluorescence (XRF, EDX-720, Shimadzu). HR-TEM and high-angle annular dark-field (HAADF) imaging along with EDS were carried out using a FEI TITAN G2 Titan microscopes, operated at 300 KeV. TEM grids were prepared by dispersing samples in ethanol (15 s ultrasonication) and then dropping onto a carbon Cu grid. Surface chemical composition and oxidation state was determined by X-ray photoelectron spectroscopy (XPS) on a Thermo Scientific Escalab 250Xi instrument using monochromated Al K_α (1486.68 eV) radiation, with a spot size of 650 μm. High-resolution XP spectra were collected at 20 eV pass energy, with binding energies referenced to the C 1 s value of adventitious carbon, which was fixed at 284.6 eV. Spectra were analyzed and quantified using CasaXPS. Raman spectra were measured on HORIBA Jobin Yvon μ-Raman spectrometer with a 532 nm Ar laser operated at 4 mW. UV–vis absorbance spectra of prepared samples and degraded dye samples were obtained using a Perkin Elmer Lambda 35 spectrometer. Photoluminescence (PL) was performed using a Perkin Elmer spectrofluorometer LS-55. Thermogravimetric analysis (TGA) was undertaken on a TA Instruments TGA Q50 under N_2 between room temperature and 800 °C using a heating rate of 10 °C/min. Specific surface areas were calculated from N_2 adsorption-desorption isotherms obtained using a Micromeritics ASAP 2020 porosimeter. Samples were outgassed in vacuo at 120 °C for 1 h.

3. Results and discussion

3.1. Catalyst characterization

Elemental surface analysis by XRF and XPS (Table S1–2) revealed the bulk and surface Ag loadings were 4 and 14 wt% respectively; since the nominal bulk Ag loading was 6.7 wt%, the former value corresponds to an impregnation efficiency of around 60%. Note that the higher surface versus bulk Ag loading is consistent with decoration of the external surface of the titania support by discrete silver nanoparticles. The crystallinity and phase of the parent TiO_2 and Ag/TiO_2 were investigated by XRD. Fig. 2a depicts XRD patterns for both materials, which were analyzed by Rietveld refinement using TOPAS software (Fig. S1). The parent TiO_2 exhibited diffraction peaks at 25.10°, 36.65°, 37.66°, 38.38°, 47.88°, 53.75°, 54.89°, 62.53°, 68.61°, 70.19°, 74.91° and 75.90° consistent tetragonal anatase (JCPDS card no. 21-1272). Calculated lattice parameters were a = 3.791 Å and c = 9.509 Å, with a volume-averaged crystallite size of 14 nm (Table S2). Ag/TiO_2 exhibited additional reflections at 38.06°, 41.23°, 64.52° and 77.44° characteristic of fcc metal (JCPDS No:89-3722) nanoparticles of 9 nm diameter. Silver doping had limited impact on the anatase support, inducing only a slight distortion of the tetragonal unit cell (Fig. 2b), with a = 3.792 Å and c = 9.518 Å, indicating intimate contact between silver and titania components (Luttrell et al., 2014; Pelaez et al., 2012; Zhou et al., 2014; Lim et al., 2014). Corresponding Raman spectra of TiO_2 (Fig. 2c) show bands at 144.5 cm^{-1} (E_g), 197.6 cm^{-1} (E_g), 397.7 cm^{-1} (B_{1g}), 517.7 cm^{-1} (A_{1g}) and 640.5 cm^{-1} (E_g), characteristic of Ti-O and Ti-O-Ti stretches of pure anatase (Khan et al., 2014a; Kumar et al., 2017; Lim et al., 2014). Silver addition did not introduce any new features, consistent with the formation of metallic Ag nanoparticles rather than any silver oxide phase, however the titania bands were shifted to higher wavenumber (Fig. 2d), possibly due to either framework substitution of trace Ag into the TiO_2 lattice, or coordination of silver cations to defect sites, in accordance with previous reports (Khan et al., 2014a; Ruiz et al., 2013; Jaafar et al., 2015; Li et al., 2014); Li et al previously observed that the Raman spectrum of sulfur doped TiO_2 was blue-shifted due to S incorporation into the TiO_2 lattice (Li et al., 2014).

The surface composition and oxidation state of TiO_2 and Ag/TiO_2 were subsequently explored by XPS. Survey spectra shown in Fig. 3a revealed the presence of surface Ti, O and C, in addition to silver for the Ag/TiO_2 sample. High resolution Ti_{2p} XP spectrum of the TiO_2 parent evidence two peaks at 463.7 and 458.0 eV due to Ti $2p_{3/2}$ and Ti $2p_{1/2}$ spin-orbit split components respectively; the binding energy separation of the components of 5.7 eV is indicative of Ti^{4+} (Khan et al., 2014a; Wang et al., 2013; Fei and Li, 2014; Singh et al., 2017; Khan et al., 2013; Sivaranjani and Gopinath, 2011; Wang and Lim, 2013; Atuchin et al., 2006). Following Ag addition, the Ti_{2p} peaks were shifted to lower binding energies of 462.3 and 456.6 eV, indicating partial reduction of the initial Ti^{4+} support surface to Ti^{3+} species (Khan et al., 2014a; Wang and Lim, 2013; Khan et al., 2013; Sivaranjani and Gopinath, 2011; Wang and

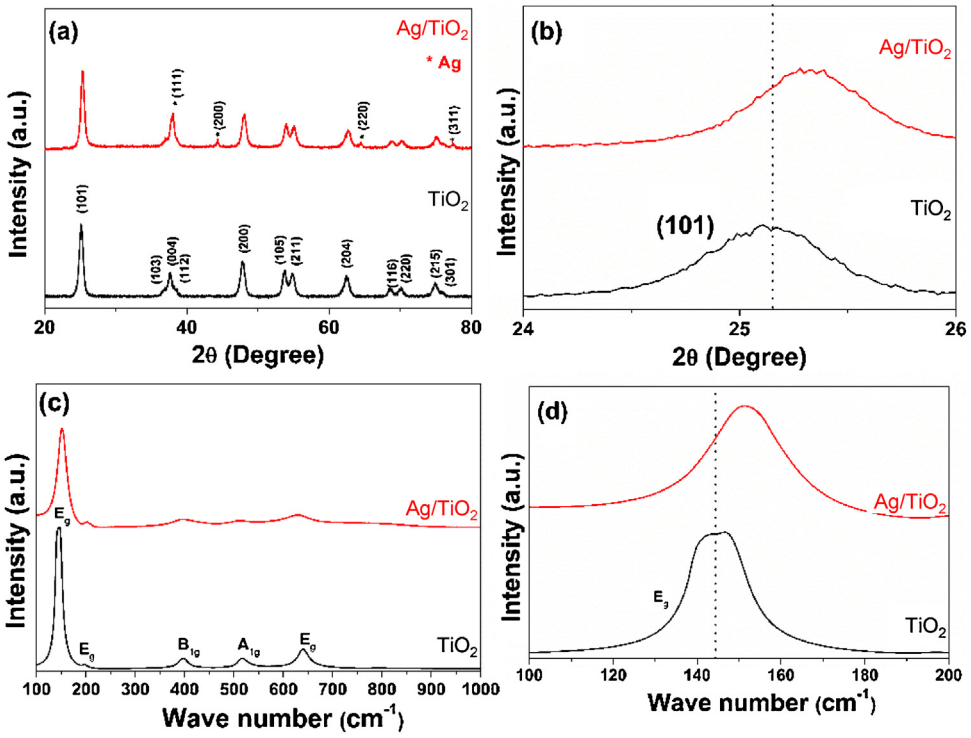

Fig. 2. (a) Wide angle powder X-ray diffraction patterns, (Saravanan et al., 2018) (b) (101) anatase powder X-ray reflection, (c) Raman spectra, and (d) principal Raman peaks of TiO_2 and Ag/TiO_2.

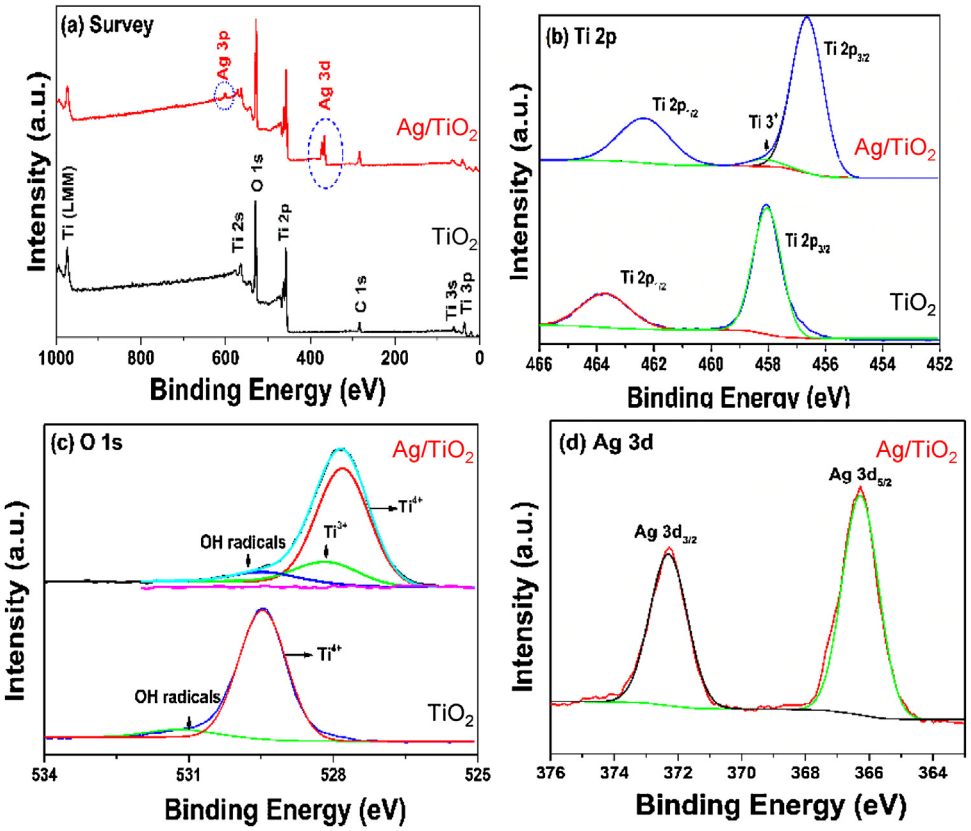

Fig. 3. XP spectra of as-prepared samples: (a) survey spectra, (b) high resolution Ti 2p spectra, (c), O 1 s spectra, (d) and Ag 3d spectrum (Saravanan et al., 2018).

Lim, 2013; Atuchin et al., 2006), demonstrating that silver incorporation induced structural/electronic perturbation of anatase as previously reported (Wang et al., 2013; Khan et al., 2013; Wang and Lim, 2013). The O 1 s XP spectrum of bare TiO_2 exhibited two chemical environments (Fig. 3c, Table S1) consistent with oxygen anions coordinated to Ti^{4+} in titania, and surface hydroxyl groups

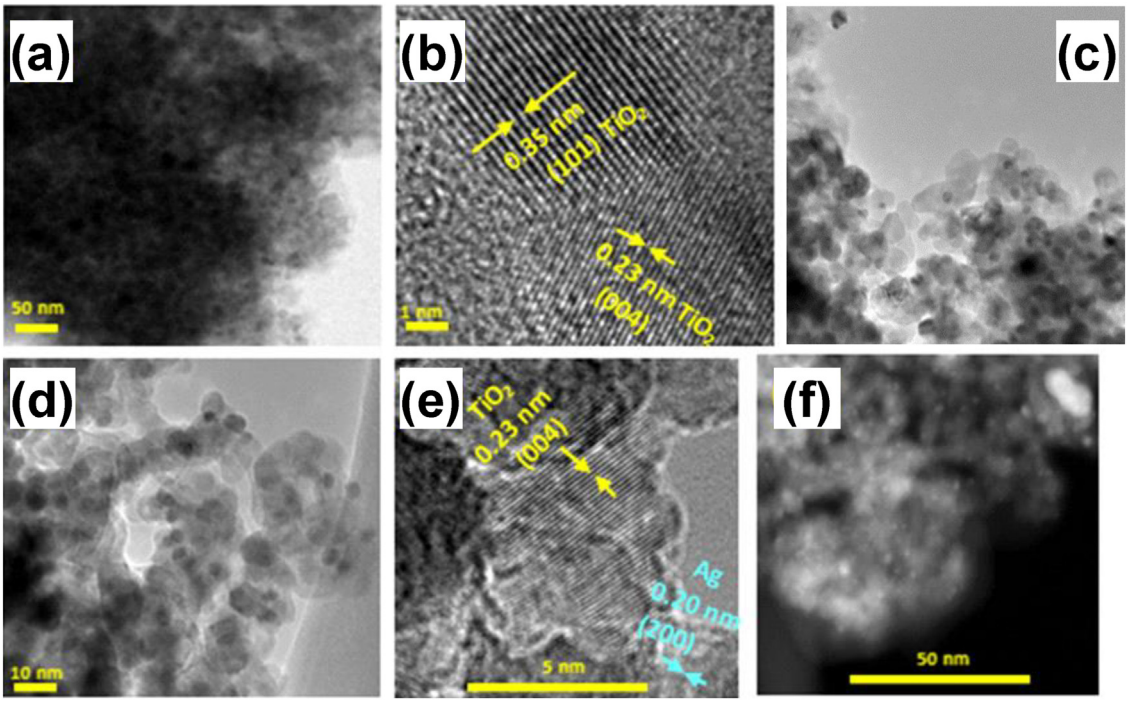

Fig. 4. (a–b) HRTEM image of TiO_2, and (c–f) HRTEM of Ag/TiO_2 (Saravanan et al., 2018).

(Khan et al., 2014a; Zhou et al., 2014; Gupta et al., 2017). Both oxygen environments shift to lower binding energy in Ag/TiO_2 (Fig. 3c), possible due to weaker charge transfer to neighbouring Ti^{3+} species (Khan et al., 2014a; Sivaranjani and Gopinath, 2011; Atuchin et al., 2006). The Ag 3d XP spectrum of Ag/TiO_2 (Fig. 3d) comprised two peaks at 366.3 and 372.3 eV due to Ag $3d_{5/2}$ and Ag $3d_{3/2}$ spin-orbit split components respectively, with the binding energy separation of 6 eV indicative of metallic Ag (Gupta et al., 2017; Atuchin et al., 2006; Jiang et al., 2013), in good agreement with XRD. Peak fitting of the TiO_2 and Ag/TiO_2 materials shown in Table S3, suggests around 10% of surface titanium atoms are reduced to Ti^{3+} in the presence of silver.

Particle morphology and size distribution were further investigated by HRTEM. Fig. 4a shows a representative image of the parent TiO_2, which comprised dense agglomerates of approximately spherical nanoparticles with mean diameters of 13–15 nm (Fig. S3). Lattice fringes and associated d-spacings of 3.52 Å and 2.37 Å (Fig. 4b) were consistent with (101) and (004) planes of tetragonal anatase, with EDS image confirming particles were composed solely of Ti and O (Fig. S4). The Ag/TiO_2 sample contained higher contrast, spherical nanoparticles of 4–6 nm diameter (Fig. S5), which appear to uniformly decorate the larger TiO_2 crystallites (Fig. 4c–d); analysis of lattice fringes in Fig. 4e reveals d-spacings consistent with the (004) plane of the tetragonal structure of anatase TiO_2 and the (200) plane of fcc Ag, and hence these smaller particles are attributed to metallic Ag nanoparticles. HAADF-STEM imaging (Fig. 4f) further evidences a uniform distribution of Ag nanoparticles across the titania, with EDS confirming the presence of solely Ti, Ag and O throughout Ag/TiO_2 (Fig. S6).

Textural properties were characterized by N_2 porosimetry. Adsorption-desorption isotherms of TiO_2 and Ag/TiO_2 are shown in Fig. 5a with corresponding textural properties summarized in Table 1. Titania exhibited a Type Ia isotherm, characteristic of monolayer adsorption over non-porous crystallites (as expected from TEM) with interparticle micropore voids. Silver addition significantly lowered the surface area, possibly due to aggregation of titania crystallites during mechanothermal processing resulting in a loss of micropore voids leaving only large interparticle mesopore voids (Fig. S7) (Jaafar et al., 2015; Navarro et al., 2009). Photophysical properties were investigated by UV–vis absorption (Fig. 5b–c) and PL (Fig. 5d), which showed Ag/TiO_2 exhibits a stronger, red-shifted absorbance than TiO_2, and correspondingly smaller band gap of 2.77 vs 3.1 eV for anatase (from Tauc plots in Fig. 5c, assuming indirect band gaps for both materials). This increase in visible absorption for Ag/TiO_2 is attributed to the silver surface plasmon resonance (Khan et al., 2014a; Wu et al., 2013; Wang and Lim, 2013). Charge transport was probed by PL spectroscopy under 330 nm excitation, with the resulting emission spectra for both samples displaying bands at 430, 461, 489 and 532 nm associated with surface recombination of charge carriers within anatase TiO_2 (Wang et al., 2013; Wu et al., 2013; Ruiz et al., 2013; Sivaranjani and Gopinath, 2011; Mercado et al., 2011). Ag addition greatly suppressed the PL emission intensity in Fig. 5d, suggesting a lower rate of electron-hole recombination, concomitant with the emergence of a new, weak emission band was at 602 nm (Gomes et al., 2017; Jaafar et al., 2015; Ansari et al., 2015). Additional insight into the separation of photogenerated electron–hole pairs in Ag/TiO_2 could be obtained from the transient photocurrent response and electrochemical impedance spectroscopy, and will be the subject of future investigations.

Table 1
Textural properties of TiO_2 and Ag/TiO_2.

Sample	Total surface area (m^2/g)	Mean mesopore volume BJH (cm^3/g)	Mean mesopore diameter (nm)
TiO_2	239	0.12	2.0
Ag/TiO_2	77	0.33	17.2

In summary, electron microscopy and XRD confirmed the formation of small (~4–9 nm) metallic silver nanoparticles uniformly decorating the surface of ~14 nm tetragonal anatase crystallites in Ag/TiO_2, whose surface contains ~10% of reduced Ti^{3+} species, and exhibits strong visible light absorption and a narrower band gap

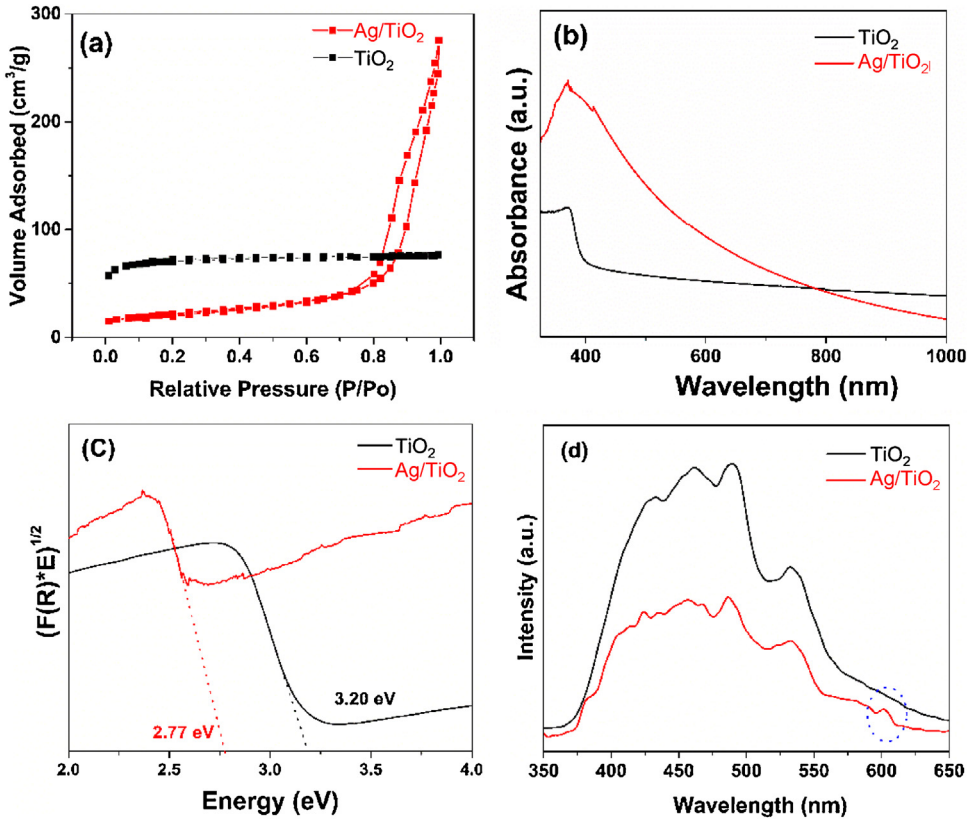

Fig. 5. (a) Nitrogen adsorption-desorption isotherms, (Saravanan et al., 2018) (b) UV–vis absorption spectra, (c) Tauc plots (indirect band gaps calculated from Kubelka Munk function), and (d) PL spectra of TiO_2 and Ag/TiO_2.

and suppressed charge carrier recombination relative to the parent titania.

3.2. Photocatalytic degradation of methyl orange (MO)

Photocatalytic degradation of MO was investigated under UV and solar irradiation TiO_2 and Ag/TiO_2, with corresponding reaction profiles shown in Fig. 6a–c. The silver doped titania significantly outperformed pure titania under both visible and solar light, with complete bleaching of MO achieved in only 80 min under simulated sunlight (Fig. 6b and c); in contrast the parent titania exhibited negligible visible photoactivity due to its wide band gap (Wang et al., 2013; Fei and Li, 2014; Ruiz et al., 2013; Khan et al., 2013; Ansari et al., 2015; Hirakawa and Kamat, 2005). The superior performance of Ag/TiO_2 is attributed to the combination of its smaller bandgap and plasmonic effects which permit visible light energy harvesting, and improved charge-carrier lifetimes evidenced by PL and previously reported (Wang et al., 2013; Fei and Li, 2014; Ruiz et al., 2013; Khan et al., 2013; Hirakawa and Kamat, 2005). The recycling performance of Ag/TiO_2 displays excellent stability for MO degradation over three recycles (Fig. 6d). The performance of our Ag/TiO_2 photocatalyst is benchmarked against related literature systems in Table S4 for the degradation of colored and colorless effluents such as phenolic compounds, methylene blue Cr (VI), reactive blue, and methyl orange under UV and visible light illumination Wang et al., 2013; Wu et al., 2013; Zhang et al., 2012; Jaafar et al., 2015; Ma et al., 2014; Fei and Li, 2014; Esfahani and Habibi, 2008; Ravishankar et al., 2015; Ansari et al., 2015; Singh et al., 2017, and MO degradation (Wang et al., 2013; Ma et al., 2014; Esfahani and Habibi 2008; Ansari et al., 2015; Singh et al., 2017). The present work evidences a significant rate enhancement for MO photodegradation (98.9% within 60 min under UV, and 99.3% within 80 min under solar irradiation corresponding to 38 $\mu mol/h/g_{cat}$). Quenching experiments were conducted to identify the reactive species responsible for MO degradation under visible light irradiation using the Ag/TiO_2 catalyst. Based on previous reports, the following quenching agents were utilized to identify the primary reactive species: ethylenediaminetetraacetic acid (EDTA) which is used to quench holes (h^+), *tert*-butyl alcohol (TBA) which quenches hydroxyl radicals ($^{\bullet}OH$), and *p*-benzoquinone which quenches oxygen species ($^{\bullet}O_2^-$) (Minero et al., 2000; Li et al., 2017; Hu et al., 2010; Dong et al., 2013). Fig. S8 suggests that h^+ and $^{\bullet}O_2^-$ species are essential for high rates of MO degradation, whereas $^{\bullet}OH$ radicals were relatively unimportant in accordance with a previous report (Dong et al., 2013).

The proposed visible light-induced photocatalytic pathway mechanism of Ag/TiO_2 for decomposition of dyes is displayed in Fig. 6e. The Ag/TiO_2 comprises metallic Ag, Ti^{3+} and Ti^{4+} states. The conduction band positions of Ti^{3+} (−4.55 eV), Ti^{4+} (−4.21 eV) and Fermi level of metallic Ag (−4.64 eV) are very close to each other (Xu and Schoonen, 2000; Chung et al., 2012; Uda et al., 1998). In short, when the metallic nanoparticles form an interface with semiconducting materials a Schottky barrier is formed, resulting in a new Fermi level (Saravanan et al., 2013; Lee et al., 2014; Zheng et al., 2008), and a high number of free electrons due to the presence of metallic Ag (Saravanan et al., 2013; Lee et al., 2014; Hohmeyer et al., 2010). Under visible light irradiation, free electrons are stimulated through the silver SPR mechanism, and can move into the conduction band of the partially reduced TiO_2 (Saravanan et al., 2013; Zheng et al., 2008). These conduction band electrons may react with adsorbed molecular oxygen to generate superoxide anions, which in turn can react with water molecules to form hydroxyl radicals; such free radicals are extremely efficient at the photodegradation of organic pollutants. The synergy between Ag and TiO_2 (and asso-

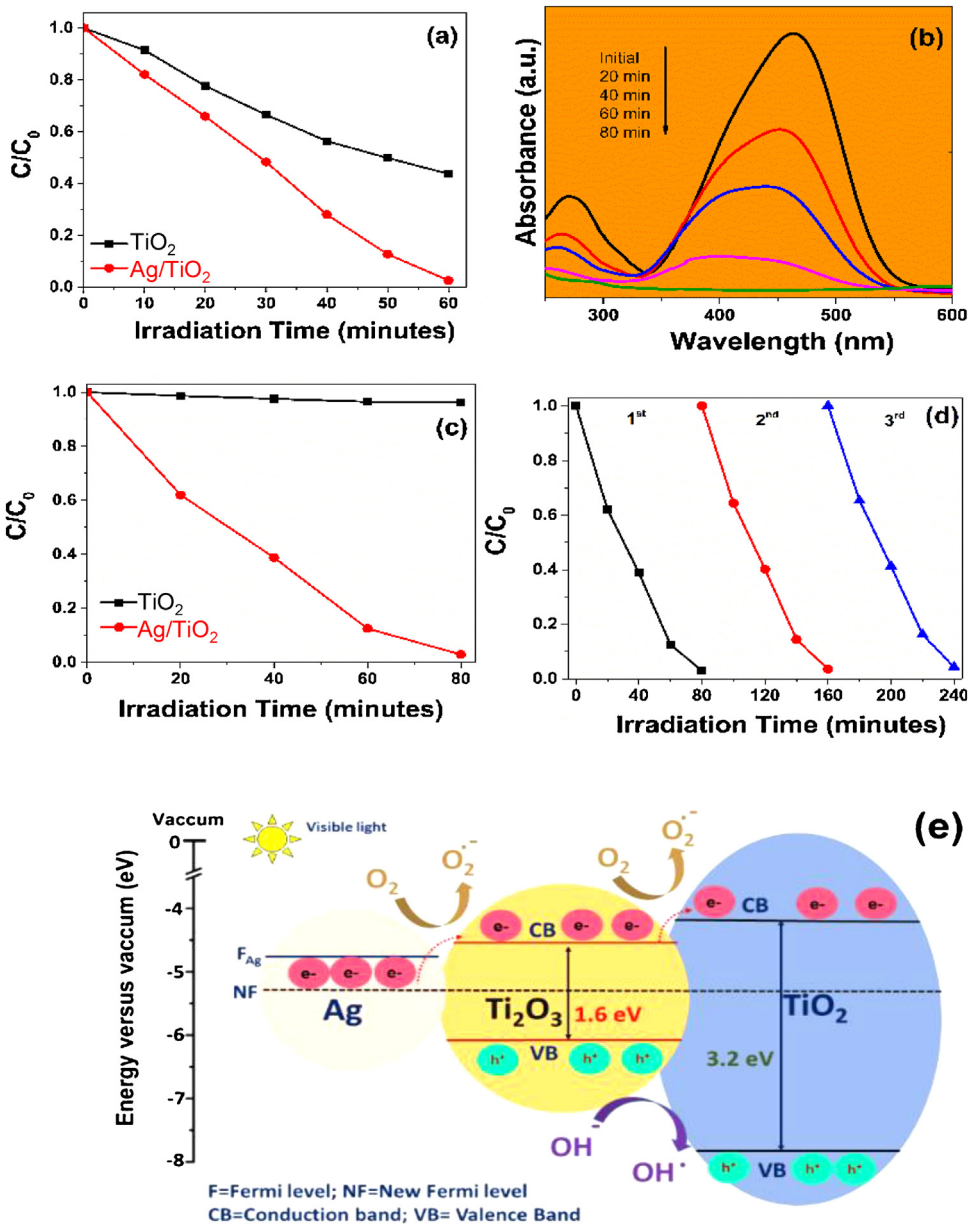

Fig. 6. Photocatalytic MO degradation under (a) UV or (b–c) simulated solar irradiation over Ag/TiO_2, (d) recycle experiments simulated solar irradiation, and (e) proposed photodegradation mechanism.

ciated Ti^{3+} formation) appears responsible for the excellent visible light performance (Khan et al., 2014a; Ansari et al., 2015; Hohmeyer et al., 2010; Khan et al., 2014b; Pan et al., 2013; Khan et al., 2014c).

3.3. *Photocatalytic hydrogen generation*

Photocatalytic hydrogen generation by water splitting was performed in the presence of methanol as a hole acceptor to increase hydrogen productivity (Wu et al., 2013; Ravishankar et al., 2015; Saravanan et al., 2014). The UV and simulated solar light photoactivity for hydrogen generation over titania and Ag/TiO_2 are shown in Fig. 7a–b. Silver addition again significantly enhanced photoactivity under UV irradiation, and dramatically increased visible photoactivity with respect to the parent titania which was essentially inert (Wu et al., 2013; Ravishankar et al., 2015; Gupta et al., 2017). As for MO photodegradation, the superior photocatalytic hydrogen production over Ag/TiO_2 is attributed to its narrower band gap, light harvesting through the silver surface plasmon resonance, and formation of intermediate states between Ag nanoparticles and Ti^{3+} defects which suppress electron-hole recombination (Wu et al., 2013; Ravishankar et al., 2015; Wang et al., 2012; Zuo et al., 2010; Zhang et al., 2014). Hydrogen productivity compares very favorably with related literature (Table S5), with Ag/TiO_2 achieving 2880 μmol/h/g_{cat} and 910 μmol/h/g_{cat} of hydrogen under UV and simulated solar light respectively, higher than previous reports (Wu et al., 2013; Ortiz et al., 2015; Lian et al., 2015; Ge et al., 2016b; Ravishankar et al., 2015).

The following mechanism is proposed for photocatalytic H_2O splitting to H_2 under solar irradiation (Wu et al., 2013; Gupta et al., 2017):

$$Ag/TiO_2 + h\nu(visiblelight) \rightarrow Ag/TiO_2(4e^- + 4h^+) \quad (1)$$

$$4h^+ + H_2O + CH_3OH \rightarrow 4H^+ + HCHO_{(g)} + \tfrac{1}{2}O_{2(g)} \quad (2)$$

$$HCHO_{(g)} + H_2O \leftrightarrow HCO_2H_{(liq)} + H_{2(g)} \quad (3)$$

$$HCO_2H_{(liq)} \leftrightarrow CO_{2(g)} + H_{2(g)} \quad (4)$$

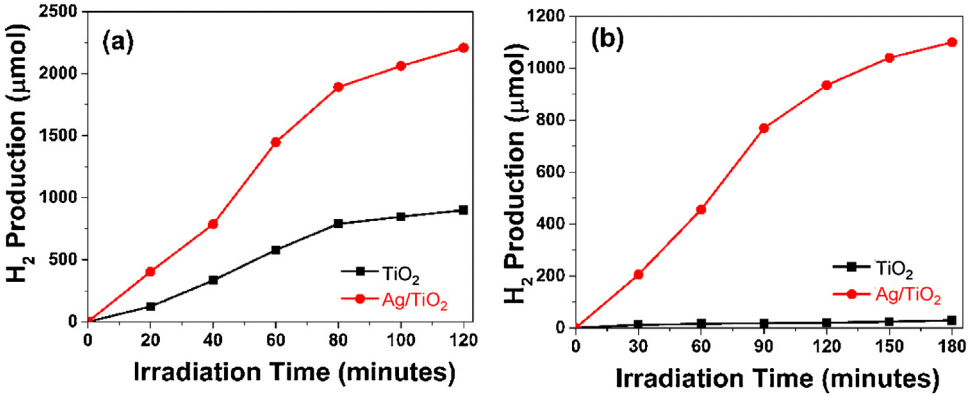

Fig. 7. Photocatalytic hydrogen generation under (a) UV light, and, (b) Visible light irradiation using prepared TiO_2 and Ag/TiO_2.

$$4H^{+}+4e^{-}\rightarrow 2H_{2(g)} \quad (5)$$

4. Conclusions

Silver promoted titania was synthesized through a stepwise sol-gel and mechanothermal decomposition method. The resulting material comprises metallic Ag nanoparticles and partially reduced anatase crystallites which exhibit a smaller band gap and stronger visible light absorption compared to a pure titania analogue. TEM and HAADF images indicate the Ag nanoparticles are homogeneously distributed over the TiO_2 surface. The combination of plasmonic and trapping effects arising from silver introduction confers superior UV, and particularly visible light photoactivity for the degradation of methyl orange and hydrogen evolution.

Acknowledgements

The authors (S.R., F.G.) acknowledge the support of CONICYT through the project CONICYT/FONDAP/15110019. The author (S.R) acknowledge FONDECYT Government of Chile (Project No.: 11170414), for the support to carry out this project.

Appendix A. Supplementary data

Supplementary material related to this article can be found, in the online version, at doi:https://doi.org/10.1016/j.psep.2018.09.015.

References

Ansari, S.A., Khan, M.M., Ansari, M.O., Cho, M.H., 2015. Silver nanoparticles and defect-induced visible light photocatalytic and photoelectrochemical performance of Ag@m-TiO_2 nanocomposite. Sol. Energy Mater. Sol. Cells 141, 162.
Atuchin, V.V., Kesler, V.G., Pervukhina, N.V., Zhang, Z., 2006. Ti 2p and O 1s core levels and chemical bonding in titanium-bearing oxides. J. Electron. Spectrosc. Relat. Phenom. 152, 18.
Awual, M.R., Hasan, M.M., 2015. Fine-tuning mesoporous adsorbent for simultaneous ultra-trace palladium(II) detection, separation and recovery. J. Ind. Eng. Chem. 25 (507).
Awual, et al., 2015a. Schiff based ligand containing nano-composite adsorbent for optical copper(II) ions removal from aqueous solutions. Chem. Eng. J. 279, 639.
Awual, et al., 2015b. Preparation of new class composite adsorbent for enhanced palladium(II) detection and recovery. Sens. Actuators, B 209, 790.
Awual, M.R., Hasan, M.M., Khaleque, M.A., Shiekh, M., 2016. Treatment of copper(II) containing wastewater by a newly developed ligand based facial conjugate materials. Chem. Eng. J. 288, 368.
Chan, Y.J., Chong, M.F., Law, C.L., Hassell, D.G., 2009. A review on anaerobic–aerobic treatment of industrial and municipal wastewater. Chem. Eng. J. 155, 1.
Chequer, et al., 2013. Textile dyes: dyeing process and environmental impact. In: Günay, M. (Ed.), Eco-Friendly Textile Dyeing and Finishing. InTech, Rijeka, Ch. 06.
Chung, I., et al., 2012. All-solid-state dye-sensitized solar cells with high efficiency. Nature 485, 486.
Dong, R., et al., 2013. AgBr@Ag/TiO_2 core–shell composite with excellent visible light photocatalytic activity and hydrothermal stability. Catal. Commun. 38, 16.
Esfahani, M.N., Habibi, M.H., 2008. Silver doped TiO_2 nanostructure composite photocatalyst film synthesized by sol-gel spin and dip coating technique on glass. Int. J. Photo Energy 2008, 628713.
Fei, J., Li, J., 2014. Controlled preparation of porous TiO_2–Ag nanostructures through supramolecular assembly for plasmon-enhanced photocatalysis. Adv. Mater. 27, 314.
Ge, M., et al., 2016a. A review of one-dimensional TiO_2 nanostructured materials for environmental and energy applications. J. Mater. Chem. A 4, 6772.
Ge, M.Z., et al., 2016b. In situ plasmonic Ag nanoparticle anchored TiO_2 nanotube arrays as visible light-driven photocatalysts for enhanced water splitting. Nanoscale 8, 5226.
Gomes, J.F., et al., 2017. Detoxification of parabens using UV-a enhanced by noble metals-TiO_2 supported catalysts. J. Environ. Chem. Eng. 5, 3065.
Gupta, V.K., et al., 2017. Degradation of azo dyes under different wavelengths of UV light with chitosan-SnO_2 nanocomposites. J. Mol. Liq. 232, 423.
Hirakawa, T., Kamat, P.V., 2005. Charge separation and catalytic activity of Ag@TiO_2 core-shell composite clusters under UV-irradiation. J. Am. Chem. Soc. 127, 3928.
Hohmeyer, J., et al., 2010. Activation of dihydrogen on supported and unsupported silver catalysts. J. Catal. 269, 5.
Hu, C., et al., 2010. Plasmon-induced photodegradation of toxic pollutants with Ag–AgI/Al_2O_3 under visible-light irradiation. J. Am. Chem. Soc. 132, 857.
Hu, W., et al., 2016. Facile strategy for controllable synthesis of stable mesoporous black TiO_2 hollow spheres with efficient solar-driven photocatalytic hydrogen evolution. J. Mater. Chem. A 4, 7495.
Jaafar, N.F., et al., 2015. Direct in situ activation of ag° nanoparticles in synthesis of Ag/TiO_2 and its photoactivity. Appl. Surf. Sci. 338, 75.
Jiang, W., Liu, H., Yin, L., Ding, Y., 2013. Fabrication of well-arrayed plasmonic mesoporous TiO_2/Ag films for dye-sensitized solar cells by multiple-step nanoimprint lithography. J. Mater. Chem. A 1, 6433.
Khan, M.M., Ansari, S.A., Amal, M.I., Lee, J., Cho, M.H., 2013. Highly visible light active Ag@TiO_2 nanocomposites synthesized using an electrochemically active biofilm: a novel biogenic approach. Nanoscale 5, 4427.
Khan, M.M., et al., 2014a. Band gap engineered TiO2 nanoparticles for visible light induced photoelectrochemical and photocatalytic studies. J. Mater. Chem. A 2, 637.
Khan, M.M., et al., 2014b. Defect-induced band gap narrowed CeO_2 nanostructures for visible light activities. Ind. Eng. Chem. Res. 53, 9754.
Khan, M.M., et al., 2014c. Electrochemically active biofilm assisted synthesis of Ag@CeO_2 nanocomposites for antimicrobial activity, photocatalysis and photoelectrodes. J. Coll. Interface Sci. 431, 255.
Kumar, S., et al., 2017. P25@CoAl layered double hydroxide heterojunction nanocomposites for CO_2 photocatalytic reduction. Appl. Catal. B Environ. 209, 394.
Lee, H., Lee, Y.K., Hwang, E., Park, J.Y., 2014. Enhanced surface plasmon effect of Ag/TiO_2 nanodiodes on internal photoemission. J. Phys. Chem. C 118, 5650.
Li, N., et al., 2014. High quality sulfur-doped titanium dioxide nanocatalysts with visible light photocatalytic activity from non-hydrolytic thermolysis synthesis. Inorg. Chem. Front. 1, 521.
Li, P., Liu, Z., Wang, X., Guo, Y., Wang, L., 2017. Enhanced decolorization of methyl orange in aqueous solution using iron-carbon micro-electrolysis activation of sodium persulfate. Chemosphere 180, 100.
Lian, Z., et al., 2015. Plasmonic silver quantum dots coupled with hierarchical TiO_2 nanotube arrays photoelectrodes for efficient visible-light photoelectrocatalytic hydrogen evolution. Sci. Rep. 5, 10461.
Lim, S.P., Pandikumar, A., Huang, N.M., Lim, H.N., 2014. Enhanced photovoltaic performance of silver@titania plasmonic photoanode in dye-sensitized solar cells. RSC Adv. 4, 38111.
Logvinenko, V., Polunina, O., Mikhailov, Y., Mikhailov, K., Bokhonov, B., 2007. Study of thermal decomposition of silver acetate. J. Therm. Anal. Cal. 90, 813.
Luttrell, T., et al., 2014. Why is anatase a better photocatalyst than rutile? - model studies on epitaxial TiO_2 films. Sci. Rep. 4, 4043.

Ma, J., et al., 2014. Fabrication of Ag/TiO_2 nanotube array with enhanced photocatalytic degradation of aqueous organic pollutant. Phys. E Low.-Dimension. Syst. Nanostruct. 58, 24.
Mercado, C., Seeley, Z., Bandyopadhyay, A., Bose, S., McHale, J.L., 2011. Photoluminescence of dense nanocrystalline titanium dioxide thin films: effect of doping and thickness and relation to gas sensing. ACS Appl. Mater. Interfaces 3, 2281.
Minero, C., Mariella, G., Maurino, V., Vione, D., Pelizzetti, E., 2000. Photocatalytic transformation of organic compounds in the presence of inorganic ions. 2. Competitive reactions of phenol and alcohols on a titanium dioxide-fluoride system. Langmuir 16, 8964.
Navarro, C.R., et al., 2009. Thermal decomposition of calcite: mechanisms of formation and textural evolution of CaO nanocrystals. Am Mineral. 94, 578.
Ortiz, A.L., et al., 2015. Silver oxidation state effect on the photocatalytic properties of Ag doped TiO_2 for hydrogen production under visible light. Int. J. Hydrogen Energy 40, 17308.
Pan, Z.W., Dai, Z.R., Wang, Z.L., 2001. Nanobelts of semiconducting oxides. Science 291, 1947.
Pan, X., Yang, M.Q., Fu, X., Zhang, N., Xu, Y.J., 2013. Defective TiO_2 with oxygen vacancies: synthesis, properties and photocatalytic applications. Nanoscale 5, 3601.
Pelaez, M., et al., 2012. A review on the visible light active titanium dioxide photocatalysts for environmental applications. Appl. Catal. B Environ. 125, 331.
Ravishankar, T.N., et al., 2015. Hydrogen generation and degradation of trypan blue using fern-like structured silver-doped TiO_2 nanoparticles. New J. Chem. 39, 1421.
Ruiz, S.O., Zanella, R., López, R., Gordillo, A.H., Gómez, R., 2013. Photocatalytic hydrogen production by water/methanol decomposition using Au/TiO2 prepared by deposition–precipitation with urea. J. Hazard. Mater. 263, 2.
Saravanan, R., et al., 2013. ZnO/Ag nanocomposite: an efficient catalyst for degradation studies of textile effluents under visible light. Mater. Sci. Eng. C 33, 2235.
Saravanan, R., Gupta, V.K., Narayanan, V., Stephen, A., 2014. Visible light degradation of textile effluent using novel catalyst ZnO/γ-Mn_2O_3. J. Taiwan Inst. Chem. Eng. 45, 1910.
Saravanan, et al., 2018. Hydrogen adsorption properties of Ag decorated TiO_2 nanomaterials. Int. J. Hydrogen Energy 43, 2861.
Singh, J., Satpati, B., Mohapatra, S., 2017. Structural, optical and plasmonic properties of Ag-TiO_2 hybrid plasmonic nanostructures with enhanced photocatalytic activity. Plasmonics 12, 877.
Sivaranjani, K., Gopinath, C.S., 2011. Porosity driven photocatalytic activity of wormhole mesoporous $TiO_{2-x}N_x$ in direct sunlight. J. Mater. Chem. 21, 2639.
Sivula, K., Krol, R., 2016. Semiconducting materials for photoelectrochemical energy conversion. Nat. Rev. Mater. 1, 15010.
Tachibana, Y., Vayssieres, L., Durrant, J.R., 2012. Artificial photosynthesis for solar water-splitting. Nat. Photonics 6, 511.
Uboncholakate, K., Sikong, L., Saito, F., 2012. Photocatalytic disinfection of P.aeruginosa bacterial Ag-doped TiO_2 film. Procedia Eng. 32, 656.
Uda, M., Nakamura, A., Yamamoto, T., Fujirnoto, Y., 1998. Work function of polycrystalline Ag, Au and Al. J. Electron. Spectrosc. Relat. Phenom. (88-92), 643.
US Energy Information Administration, 2016. Retrieved on July 15th, 2016. https://www.eia.gov/forecasts/aeo/section_elecgeneration.cfm.
Wang, X., Lim, T.T., 2013. Highly efficient and stable Ag-AgBr/TiO_2 composites for destruction of Escherichia coli under visible light irradiation. Water Res. 47, 4148.
Wang, P., et al., 2012. Lattice defect-enhanced hydrogen production in nanostructured hematite-based photoelectrochemical device. ACS Appl. Mater. Interfaces 4, 2295.
Wang, S., et al., 2013. Facile one-pot synthesis of uniform TiO_2–Ag hybrid hollow spheres with enhanced photocatalytic activity. Dalton Trans. 42, 1122.
Wang, Q., et al., 2016. Scalable water splitting on particulate photocatalyst sheets with a solar-to-hydrogen energy conversion efficiency exceeding 1%. Nat. Mater. 15, 611.
World Health Organization WHO, 2017. Global Health Observatory Data Repository. WHO, World Health Organization, pp. 2016.
Wu, F., et al., 2013. Photocatalytic activity of Ag/TiO_2 nanotube arrays enhanced by surface plasmon resonance and application in hydrogen evolution by water splitting. Plasmonics 8, 501.
Xu, Y., Schoonen, M.A.A., 2000. The absolute energy positions of conduction and valence bands of selected semiconducting minerals. Am Mineral. 85, 543.
Yan, J., et al., 2013. Understanding the effect of surface/bulk defects on the photocatalytic activity of TiO_2: anatase versus rutile. Phys. Chem. Chem. Phys. 15, 10978.
Zhang, H., et al., 2012. Defect-mediated formation of Ag cluster-doped TiO_2 nanoparticles for efficient photodegradation of pentachlorophenol. Langmuir 28, 3938.
Zhang, Z., et al., 2014. Direct evidence of plasmon enhancement on photocatalytic hydrogen generation over Au/Pt-decorated TiO_2 nanofibers. Nanoscale 6, 5217.
Zheng, Y., et al., 2008. Photocatalytic activity of Ag/ZnO heterostructurenanocatalyst: correlation between structure and property. J Phys. Chem. C 112, 10773.
Zhou, W., et al., 2011. Well-ordered large-pore mesoporous anatase TiO_2 with remarkably high thermal stability and improved crystallinity: preparation, characterization, and photocatalytic performance. Adv. Funct. Mater. 21, 1922.
Zhou, W., et al., 2014. Ordered mesoporous black TiO_2 as highly efficient hydrogen evolution photocatalyst. J. Am. Chem. Soc. 136, 9280.
Zuo, F., et al., 2010. Self-doped Ti^{3+} enhanced photocatalyst for hydrogen production under visible light. J. Am. Chem. Soc. 132, 11856.